processes

MDPI

Article

Electrochemical Tuning of Ni-Fe Catalysts Using Various Techniques for Efficient Hydrogen Evolution in Alkaline Media

Ali Topak [1] and Serap Toprak Döşlü [2,*]

[1] Department of Chemistry, Institute for Graduate Education, Mardin Artuklu University, Mardin 47100, Türkiye
[2] Department of Nutrition and Dietetics, Faculty of Health Sciences, Mardin Artuklu University, Mardin 47100, Türkiye
* Correspondence: seraptoprak@artuklu.edu.tr; Tel.: +90-(482)-2121395-7251

Abstract: The search for cost-effective and scalable electrocatalysts for the hydrogen evolution reaction (HER) remains a critical challenge in advancing sustainable energy technologies. This study presents a novel approach to optimizing nickel-iron (Ni-Fe) alloy coatings on graphite (G) electrodes through a strategic combination of composition tuning, nickel modification, and various electrochemical optimizations. Unlike conventional studies, which primarily focus on static alloy compositions, this work systematically investigates the impact of dynamic nickel modification durations on the catalytic performance and conductivity of Ni-Fe alloys. By addressing the conductivity limitations caused by iron oxidation, the study demonstrates the enhanced HER kinetics achieved with a Ni-modified G/$Ni_{\%95}Fe_{\%5}$-Ni(60s) electrode. Electrochemical and structural analyses reveal the synergistic effects of nickel modifications on improving active site accessibility, reducing overpotential, and increasing hydrogen production efficiency. This work introduces a scalable methodology for tailoring Ni-Fe catalysts, offering significant advancements in the development of robust, cost-effective electrocatalysts for industrial-scale hydrogen production.

Keywords: Ni-Fe coatings; Ni modified; electrocatalyst; HER; alkaline electrolysis

check for updates

Academic Editor: Mariana de Mattos V. M. Souza

Received: 31 December 2024
Revised: 31 January 2025
Accepted: 19 February 2025
Published: 25 February 2025

Citation: Topak, A.; Toprak Döşlü, S. Electrochemical Tuning of Ni-Fe Catalysts Using Various Techniques for Efficient Hydrogen Evolution in Alkaline Media. *Processes* **2025**, *13*, 644. https://doi.org/10.3390/pr13030644

Copyright: © 2025 by the authors. Licensee MDPI, Basel, Switzerland. This article is an open access article distributed under the terms and conditions of the Creative Commons Attribution (CC BY) license (https://creativecommons.org/licenses/by/4.0/).

1. Introduction

Hydrogen energy stands out as a sustainable alternative to fossil fuels, playing a crucial role in mitigating the escalating global concerns surrounding carbon emissions and climate change. The combustion of fossil fuels is a major contributor to atmospheric greenhouse gas concentrations, leading to adverse environmental impacts. In contrast, hydrogen offers a clean energy pathway, with the potential for near-zero carbon emissions throughout its lifecycle, depending on the production method employed [1,2]. The transition to a hydrogen-based economy is therefore essential to achieve the global decarbonization goals and mitigate the effects of climate change [3,4]. Besides its environmental benefits, hydrogen also boasts high energy density and other environmentally friendly characteristics [5–8]. Among the various hydrogen production methods, water electrolysis is a particularly promising approach for generating clean hydrogen energy [9–13]. However, challenges such as a high energy consumption and overpotential losses during electrolysis significantly limit its efficiency [14–17]. Addressing these issues requires the development of cost-effective and high-performance electrocatalysts [18–23].

Transition metals such as nickel (Ni) and iron (Fe) are among the most effective and economical catalysts for the hydrogen evolution reaction (HER) [24,25]. Nickel, with its excellent electrical conductivity and chemical stability, is widely employed in HER

applications. Iron, despite its lower intrinsic activity, contributes synergistically to Ni based catalysts due to its low cost, earth abundance, and ability to modify the electronic structure of nickel [26–28]. Ni-Fe alloys combine the advantages of both metals, demonstrating superior catalytic activity and durability compared to their individual counterparts [29,30].

The synthesis of Ni-Fe catalysts can be achieved through various methods, each influencing the final morphology, composition, and thus, the catalytic performance. Common techniques include electrodeposition [31], hydrothermal synthesis [32], and chemical reduction [33]. Electrodeposition offers precise control over film thickness and composition, making it a popular choice for preparing Ni-Fe coatings on conductive substrates. Hydrothermal methods facilitate the formation of nanostructured materials with high surface areas, while a chemical reduction allows for the scalable production of catalyst powders.

The Ni/Fe ratio plays a crucial role in determining the catalytic activity of these alloys. Studies have revealed a volcano-type relationship between the Ni/Fe ratio and HER performance [34]. An optimal Ni/Fe ratio is essential to balance the hydrogen adsorption energy, which is a key descriptor for HER activity. For example, a recent study showed that a Ni/Fe ratio of [35] exhibited the highest HER activity due to the synergetic effects between nickel and iron. Specifically, the presence of iron alters the adsorption geometry on the catalyst surface, thereby optimizing hydrogen adsorption and enhancing charge transfer processes. Furthermore, the incorporation of iron can lead to the formation of iron oxyhydroxides (FeOOH) during the HER process, which can further enhance catalytic activity [36]. Optimizing the Ni/Fe ratio, along with controlling the morphology and crystalline structure of the alloy, is therefore critical for maximizing HER performance [37–39].

Graphite, as a catalyst support material, has been widely used in HER due to its low cost, large surface area, high conductivity, and excellent corrosion resistance [40–42]. The ability to uniformly deposit metal coatings on graphite surfaces increases the active surface area, thereby accelerating HER kinetics [43,44]. Furthermore, electrochemical deposition methods provide a versatile and cost-effective approach to applying various metal alloys onto graphite surfaces [38].

Recent studies have demonstrated that Ni-Fe alloys not only exhibit a high performance in HER, but also significant catalytic activity for oxygen evolution reactions (OER), primarily due to the synergistic effects between Ni and Fe atoms [39]. The close atomic radii of these elements strengthen the alloy structure and facilitate charge transfer at the catalyst surface. Literature reports suggest that varying the composition and morphology of Ni-Fe alloys can optimize their catalytic performance [40,41].

In this study, a low-cost, high-performance, and structurally stable electrocatalyst was developed by coating a graphite electrode with a Ni-Fe alloy and subsequently modifying the surface with nickel for different durations. The catalytic activities of the prepared electrodes for HER were evaluated using electrochemical methods such as electrochemical impedance spectroscopy (EIS), linear sweep voltammetry (LSV), and cyclic voltammetry (CV). Additionally, surface morphology and chemical composition were characterized by a scanning electron microscopy (SEM), energy dispersive X-ray spectroscopy (EDX), and X-ray diffraction (XRD). The primary objective of this study was to determine the optimal composition of the Ni-Fe alloy and identify the nickel modification duration that enhances HER performance while maintaining structural stability.

2. Materials and Methods

2.1. Preparation of Ni-Fe Coated Electrodes

Electrochemical deposition was used to coat a graphite electrode (0.283 cm^2) with Ni-Fe alloys of varying compositions. The electrolyte bath consisted of $NiSO_4 \cdot 6H_2O$ and

$FeSO_4 \cdot 7H_2O$. Six different Ni-Fe ratios were prepared, ranging from 99–1% to 95–5%. The deposition was performed at a constant current density of 14.15 mA/cm^2 and a temperature of 298 K. The electrolyte bath consisted of $NiSO_4 \cdot 6H_2O$ and $FeSO_4 \cdot 7H_2O$. Six different Ni-Fe ratios were prepared, ranging from 99–1% to 95–5%. Additionally, a $G/Ni_{\%93}Fe_{\%7}$ composition was prepared to investigate the effects of higher iron content on catalytic performance. Deposition times for each composition were calculated using Faraday's law.

Prior to the deposition, the graphite electrodes were polished with sandpaper to ensure a clean and uniform surface. The electrodeposition setup used a three-electrode system: the graphite electrode served as the working electrode, and the platinum electrodes (2 cm^2) and the Ag/AgCl electrode were used as the counter and reference electrodes, respectively.

2.2. Electrochemical Analysis of Ni-Fe Electrodes

After the deposition, the resulting electrodes ($G/Ni_{\%99}Fe_{\%1}$, $G/Ni_{\%98}Fe_{\%2}$, $G/Ni_{\%97}Fe_{\%3}$, $G/Ni_{\%96}Fe_{\%4}$, $G/Ni_{\%95}Fe_{\%5}$, and $G/Ni_{\%93}Fe_{\%7}$) were tested in a 1.0 M KOH solution at room temperature. Electrochemical impedance spectroscopy (EIS), linear sweep voltammetry (LSV), and cyclic voltammetry (CV) techniques were used to evaluate the catalytic performance. Among these, the $G/Ni_{\%95}Fe_{\%5}$ electrode exhibited the best catalytic performance.

2.3. Nickel Modification of Ni-Fe Coated Electrodes

The Ni coating on the Ni-Fe alloy mitigates the conductivity reduction caused by the easy oxidation of iron, providing a more uniform and stable conductive layer that facilitates an improved charge transfer during the hydrogen evolution reaction. This modification was achieved by electrodepositing nickel from a solution containing 15 g of $NiSO_4 \cdot 6H_2O$ and 0.625 g of H_3BO_3 in 50 mL of water. The deposition was carried out at 14.15 mA/cm^2 and 298 K for durations of 30, 60, and 75 s.

The selection of deposition times (30, 60, 75 s) was informed by both preliminary experimental results and insights from the existing literature. Short deposition durations, such as 30 s, were chosen to examine the formation of initial thin layers and their influence on catalytic activity. Studies have shown that thinner nickel coatings can enhance active site exposure, thereby improving hydrogen evolution reaction (HER) performance [42].

An intermediate deposition time of 60 s was selected to achieve a balance between adequate surface coverage and the preservation of active sites, which is crucial for optimal HER kinetics. Research indicates that moderate coating thicknesses can provide sufficient conductivity while maintaining catalytic efficiency [45].

A longer deposition time of 75 s was included to assess the effects of thicker layers, such as potential increases in film resistance due to diffusion limitations or the obstruction of active sites. Excessive coating thickness has been reported to hinder ion diffusion and reduce the availability of catalytic sites, negatively impacting HER performances [46].

The modified electrodes were labeled as $G/Ni_{\%95}Fe_{\%5}$-Ni(30s), $G/Ni_{\%95}Fe_{\%5}$-Ni(60s), and $G/Ni_{\%95}Fe_{\%5}$-Ni(75s), respectively.

The $G/Ni_{\%95}Fe_{\%5}$-Ni(60s) electrode, which showed superior catalytic activity, was further treated under two specific conditions.

2.4. Electrochemical Treated Techniques of Catalysts

Nickel oxyhydroxide is known as the most efficient type of nickel derivative for the hydrogen evolution reaction. To oxidize the nickel in our catalysts, different electrochemical techniques were tested to determine the most effective method.

Cyclic Voltammetry (CV): Subjected to 50 cycles at a scan rate of 100 mV/s in the range of −1.0 V to 0.5 V.
Chronoamperometry (CA): Maintained at a potential of 0.4 V for 1800 s.

These electrodes were denoted as G/$Ni_{\%95}Fe_{\%5}$-Ni(60s)(CV) and G/$Ni_{\%95}Fe_{\%5}$-Ni(60s)(CA).

2.5. Electrochemical Characterization

All prepared electrodes were analyzed using the following techniques in a three-electrode configuration:

EIS: Frequency range of 10^5 to 10^{-1} Hz with an amplitude of 5 mV.
LSV: Scan rate of 1.0 mV/s in the potential range of −1.0 V to −1.8 V.
CV: −1.0 V to 0.5 V at scan rate of 50 mV/s.

Measurements were carried out using a Gamry Instruments Reference 3000 device. The working, reference, and counter electrodes were the prepared electrocatalyst, Ag/AgCl (3M KCl), and platinum plate (2 cm^2), respectively.

2.6. Hydrogen Evolution Measurements

The G, G/$Ni_{\%95}Fe_{\%5}$, and G/$Ni_{\%95}Fe_{\%5}$-Ni(60s) electrodes were tested for hydrogen evolution by electrolysis at a constant potential of 3 V for 1 h in 1 M KOH solution. The evolved hydrogen gas was measured using an inverted burette setup. In these experiments, the electrocatalysts acted as the cathode, while the platinum plate (2 cm^2) served as the anode.

2.7. Surface and Structural Characterization

The surface morphology of the electrodes was examined using scanning electron microscopy (SEM; JEOL JSM 6510), while their chemical composition was analyzed via energy dispersive X-ray spectroscopy (EDX). The phase structure of the electrodes was characterized using X-ray diffraction (XRD; RIGAKU ULTIMA IV) with diffraction angles ranging from 3° to 90°.

3. Result and Discussion

3.1. Electrochemical Behavior

In general, the electrocatalysts prepared by depositing Ni-Fe at different composition ratios on the graphite electrode exhibited a higher catalytic activity compared to the bare graphite electrode. When we examine the Ni-Fe coated graphite electrocatalysts among themselves, we can say that the coating activities change depending on the chemical composition ratios, and this change is clearly seen in the Nyquist and cathodic current potential curves. The G/$Ni_{\%95}Fe_{\%5}$ electrode had the lowest resistance, the least overpotential (low initial potential) and the highest current (Figure 1). By depositing Ni on this electrode for 30, 60, and 75 s, the aim was to further enhance the catalytic activity and determine the optimal Ni deposition time. Electrochemical measurements show that the G/$Ni_{\%95}Fe_{\%5}$-Ni(60s) electrode gives better results in terms of performance than the other coating times and the G/$Ni_{\%95}Fe_{\%5}$ electrode (Figure 2). This situation shows that G/$Ni_{\%95}Fe_{\%5}$ electrode is an electrode suitable for development. In addition, Ni depositions by applying a 14.15 mA current in a short time, such as 60 s, and includes significant parametric gains in terms of energy and time. With a Ni deposition of over 60 s, the layer thickness deposited on the G/$Ni_{\%95}Fe_{\%5}$ electrode surface increased with the extension of the coating time. This thickness increased the film resistance by affecting the ion diffusion at the electrode-solution interface and by closing the active centers [44]. It has also been reported that an increase in the coating thickness can negatively affect the mechanical properties of the film layer [47]. In addition to these studies, when the electrochemical analyses of G/$Ni_{\%95}Fe_{\%5}$-Ni(60s)(CV) and G/$Ni_{\%95}Fe_{\%5}$-Ni(60s)(CA) electrocatalysts obtained from G/$Ni_{\%95}Fe_{\%5}$-Ni(60s) electrode were performed, the lower potential formed in

the G/$Ni_{\%95}Fe_{\%5}$-Ni(60s)(CV) electrode, at the same overvoltage, shows that its catalytic properties are better than other electrocatalysts (Figure 3, Table 1).

Table 1. Polarization resistance of electrodes.

Electrode	R_p/Ω
Graphite(G)	439.000
G/$Ni_{\%99}Fe_{\%1}$	22.080
G/$Ni_{\%98}Fe_{\%2}$	10.350
G/$Ni_{\%97}Fe_{\%3}$	12.060
G/$Ni_{\%96}Fe_{\%4}$	4.534
G/$Ni_{\%95}Fe_{\%5}$	3.775
G/$Ni_{\%95}Fe_{\%5}$-Ni(30s)	3.703
G/$Ni_{\%95}Fe_{\%5}$-Ni(60s)	3.366
G/$Ni_{\%95}Fe_{\%5}$-Ni(75s)	12.490
G/$Ni_{\%95}Fe_{\%5}$-Ni(60s)(CA)	8.132
G/$Ni_{\%95}Fe_{\%5}$-Ni(60s)(CV)	3.100

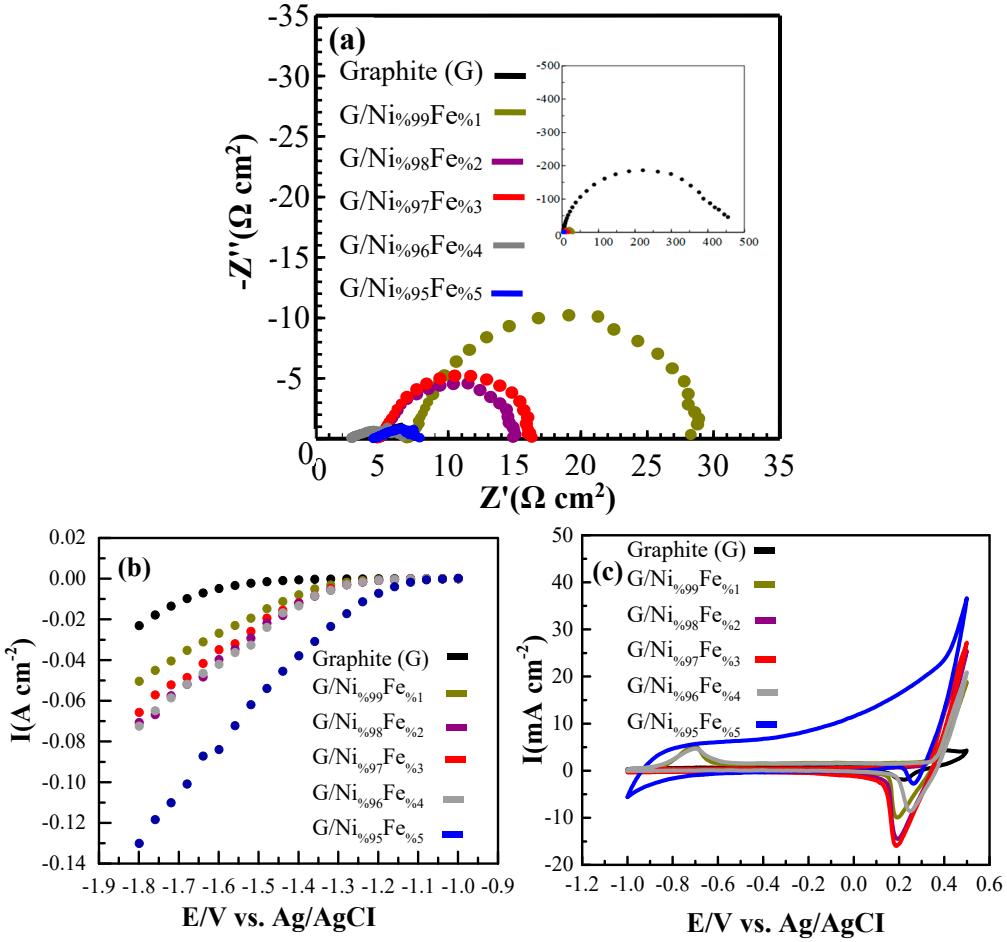

Figure 1. Nyquist curves (**a**), the current-potential curves (**b**) and the cyclic voltammograms (**c**) for G, G/$Ni_{\%99}Fe_{\%1}$, G/$Ni_{\%98}Fe_{\%2}$, G/$Ni_{\%97}Fe_{\%3}$, G/$Ni_{\%96}Fe_{\%4}$ and G/$Ni_{\%95}Fe_{\%5}$ in 1 M KOH solution at 298 K.

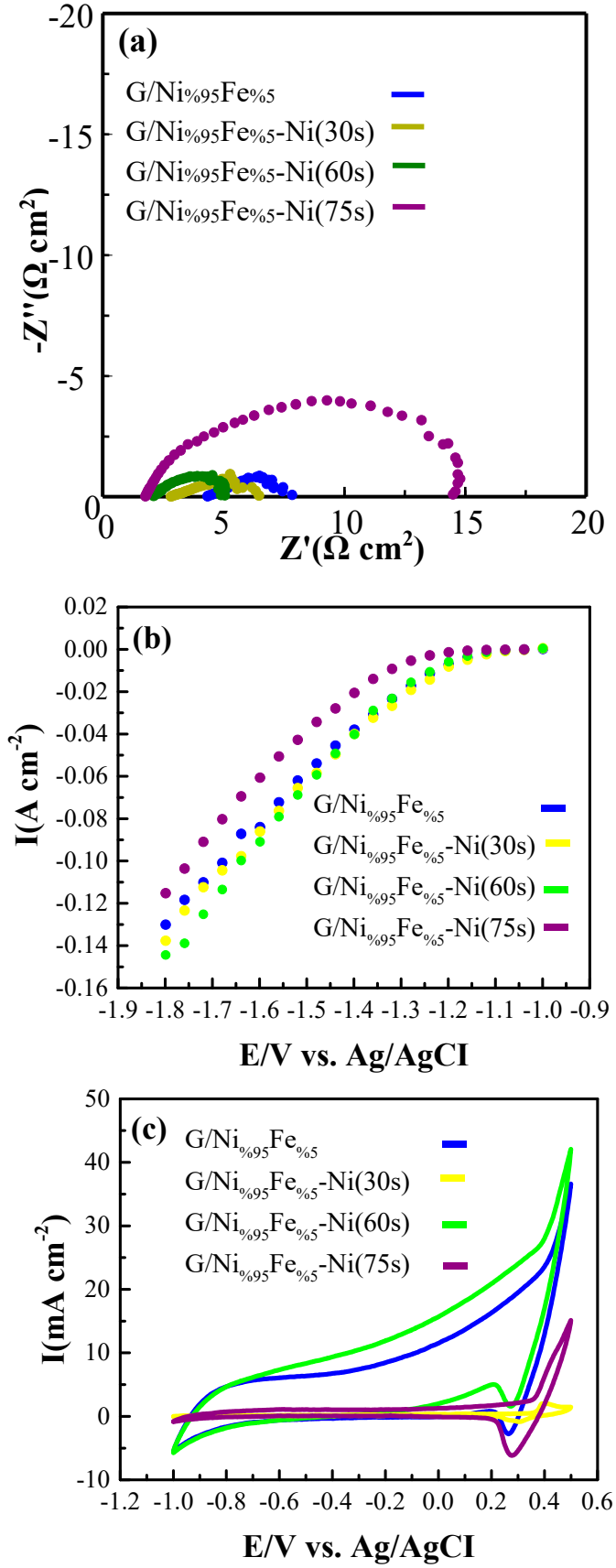

Figure 2. Nyquist curves (**a**), the current potential curves (**b**) and the cyclic voltammograms (**c**) for G/Ni$_{\%95}$Fe$_{\%5}$, G/Ni$_{\%95}$Fe$_{\%5}$-Ni(30s), G/Ni$_{\%95}$Fe$_{\%5}$-Ni(60s), and G/Ni$_{\%95}$Fe$_{\%5}$-Ni(75s) in 1 M KOH solution at 298 K.

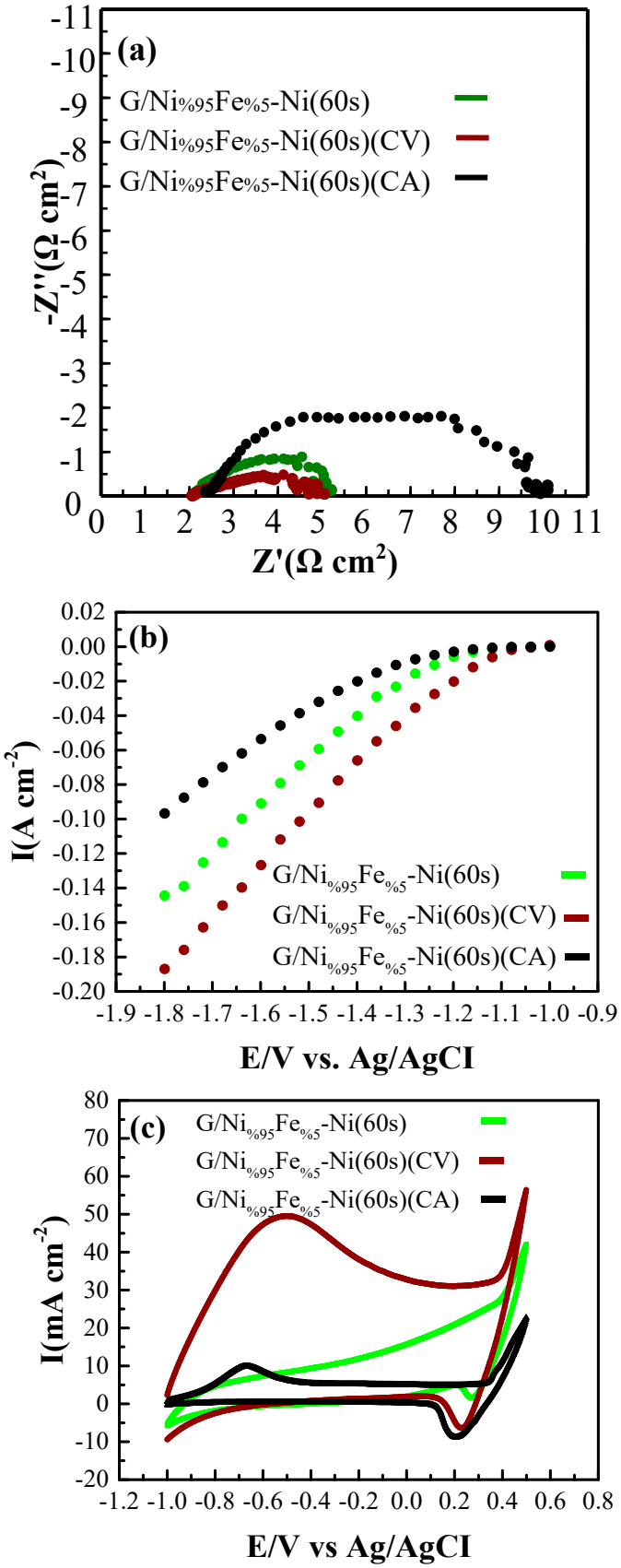

Figure 3. Nyquist curves (**a**), the current potential curves (**b**), and the cyclic voltammograms (**c**) for G/Ni%95Fe%5-Ni(60s), G/Ni%95Fe%5-Ni(60s)(CA), and G/Ni%95Fe%5-Ni(60s)(CV) in 1 M KOH solution at 298 K.

When the hydrogen gas production capabilities of G, G/Ni%95Fe%5, G/Ni%95Fe%5-Ni(60s), and G/Ni%95Fe%5-Ni(60s)(CV) electrodes were examined, parallelism with the electrochemical measurements was observed (Figure 4). The increase in current and the decrease in system resistance in ion and electron mobility provided a decrease in the overvoltage required for hydrogen production. The hydrogen gas volumes produced at G, G/Ni%95Fe%5, G/Ni%95Fe%5-Ni(60s), and G/Ni%95Fe%5-Ni(60s)(CV) electrodes were 23.2, 33.9, 72.7, and 82.8 mL, respectively (Figure 4). In fact, the hydrogen produced by the obtained G/Ni%95Fe%5-Ni(60s)(CV) electrocatalyst was approximately 3.5 times more than that produced by the bare graphite electrode. This is an important value in terms of improving electrocatalyst performance.

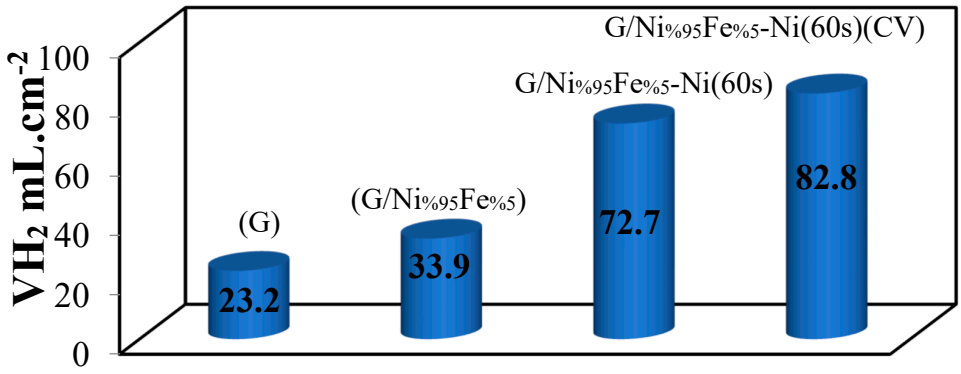

Figure 4. Released hydrogen gas in 1 h at a potential of 3 V for G, G/Ni%95Fe%5, G/Ni%95Fe%5-Ni(60s), and G/Ni%95Fe%5-Ni(60s)(CV) in a 1 M KOH solution at 298 K.

3.2. Surface Analysis

All SEM images of G, G/Ni%95Fe%5, G/Ni%95Fe%5-Ni(60s), and G/Ni%95Fe%5-Ni(60s)(CV) electrodes were obtained under the same conditions (magnitude 2000× and 10 µm) and are shown in Figure 5. When Figure 5a,b are examined, the porous structure of the graphite electrode surface and the homogeneous distribution of porosities on the surface are seen. When Figure 5c,d are examined, it is apparent that the Ni-Fe alloy is distributed tightly stacked in a spherical structure on the graphite surface, except for nano-level voids, and presents a porous structure. The approximate size of these spheres is around 1.1 µm on average (sphere sizes vary between approximately 0.6–1.3 µm). When Figure 5e,f are examined, it is seen that the surface morphology changes with the deposition of Ni on the G/Ni%95Fe%5 electrode, the surface is covered with Ni, and the surface is smooth except for small irregular grains and micro-level lines on the surface. A similar surface morphology has also been reported in the literature [48]. When Figure 5g,h are examined, it is seen that the micro lines seen on the G/Ni%95Fe%5-Ni(60s) surface disappear, the surface shows a smoother structure, and nanomolecules that cannot be measured in micro-scale are obtained. SEM images revealed that larger surface areas were formed in other electrodes coated with Ni-Fe alloy, compared to the bare graphite surface, and the G/Ni%95Fe%5-Ni(60s)(CV) electrode presented the highest 3D surface morphology. The porosity of the G/Ni%95Fe%5-Ni(60s)(CV) electrode provided a larger current density parallel to the smaller diffuse layer thickness.

The EDX images of the G, G/Ni%95Fe%5, G/Ni%95Fe%5-Ni(60s) and G/Ni%95Fe%5-Ni(60s)(CV) electrodes are shown in Figure 6. It was confirmed that the graphite surface was coated with Ni-Fe alloy and compliance with the SEM data was observed. For example, the presence of carbon atoms in the EDX findings of the G/Ni%95Fe%5-Ni(60s) electrode is attributed to the underlying graphite layer, due to the micro cracks seen in the SEM analysis. Although there are carbon atoms originating from the underlying graphite layer in the G/Ni%95Fe%5-Ni(60s)(CV) electrode, it is observed that the Ni-Fe percentage increases.

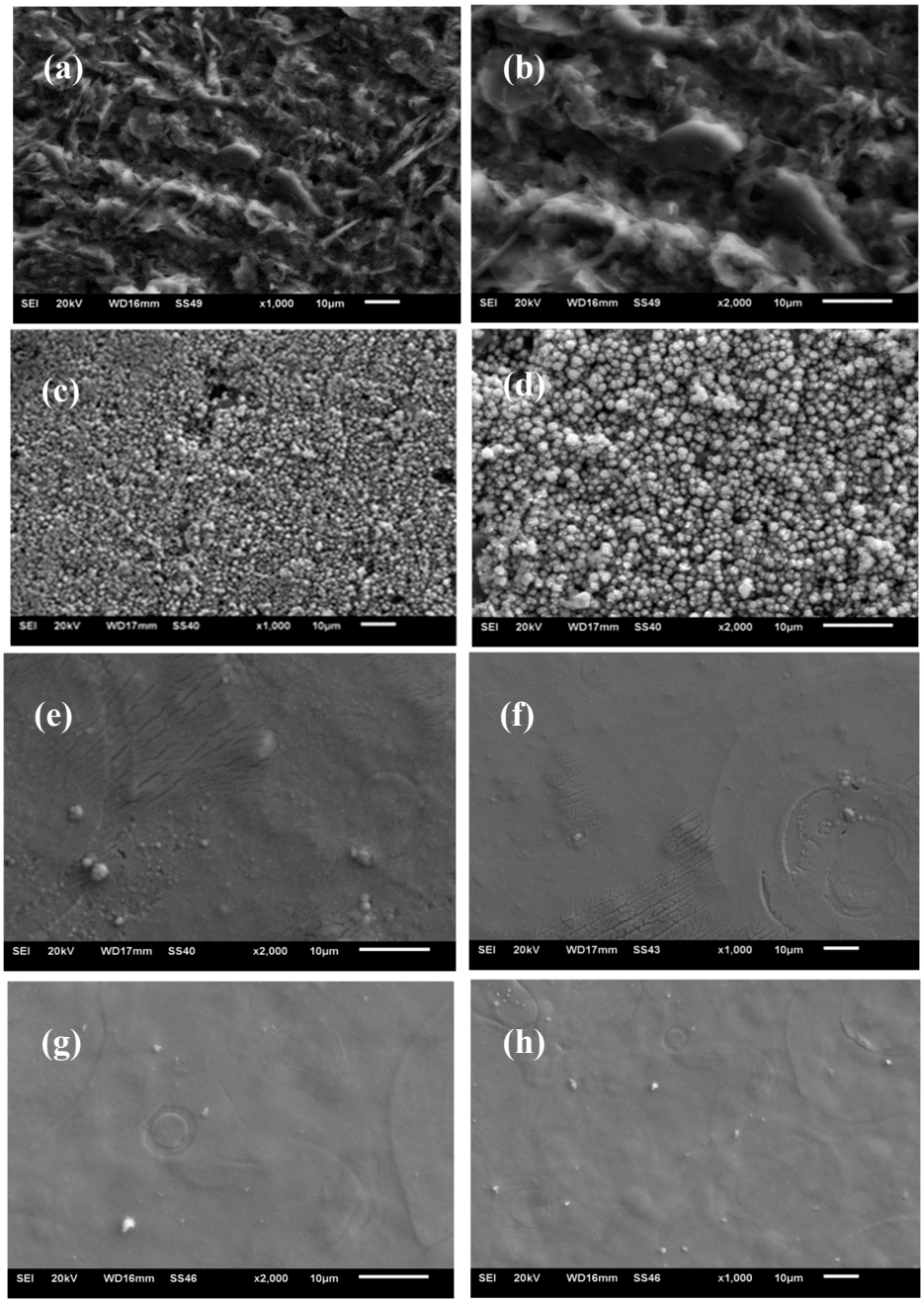

Figure 5. SEM images of G (**a**,**b**), G/$Ni_{\%95}Fe_{\%5}$ (**c**,**d**), G/$Ni_{\%95}Fe_{\%5}$-Ni(60s) (**e**,**f**), and G/$Ni_{\%95}Fe_{\%5}$-Ni(60s)(CV) (**g**,**h**) of electrodes (20 kV, 10 μm and 2000×–1000×).

The XRD results obtained for G/$Ni_{\%95}Fe_{\%5}$, G/$Ni_{\%95}Fe_{\%5}$-Ni(60s) and G/$Ni_{\%95}Fe_{\%5}$-Ni(60s)(CV) electrodes with 3° to 90° diffraction are shown in Figure 7. The XRD pattern of the G/$Ni_{\%95}Fe_{\%5}$ electrode exhibits reflections corresponding to the (111), (200), and (220) planes of a face-centered cubic structure, indicating the presence of nickel and iron. The observed peaks are located at 2θ values of [44.0°], [51.2°], and [75.5°], respectively. These reflections are consistent with the formation of a Ni-Fe alloy phase [49] [JCPDS card number: 00-047-1417]. The close atomic radii of nickel (0.124 nm) and iron (0.126 nm) atoms give the appearance of an alloyed and indistinguishable solid solution, which is why the iron peak alone is not seen [37]. The shift in the reflection (200 and 220) peaks at the G/$Ni_{\%95}Fe_{\%5}$ electrode is related to the structure of the alloy. In addition, the presence of different phases is consistent with the oxidation seen in the EDX results. Figure 7 represents XRD pattern of G/$Ni_{\%95}Fe_{\%5}$, G/$Ni_{\%95}Fe_{\%5}$-Ni(60s), and G/$Ni_{\%95}Fe_{\%5}$-Ni(60s)(CV) of

electrodes. While the nickel (111) reflection peak is observed at the G/$Ni_{\%95}Fe_{\%5}$-Ni(60s) electrode, the complete disappearance of the nickel (200 and 220) reflections is related to the presence of an amorphous model [48]. The XRD pattern of the G/$Ni_{\%95}Fe_{\%5}$-Ni(60s)(CV) electrode corresponds to the reference nickel and a well-defined nickel (111) peak indicates that the coating is crystalline. The recorded peaks correspond to the (111), (200) and (220) reflections of the face-centered cubic structure of nickel in the order of increasing 2θ [48]. Nickel (111), (200), and (220) peaks due to the alloy structure are slightly displaced. The broad peaks in the G/$Ni_{\%95}Fe_{\%5}$-Ni(60s)(CV) electrode compared to the other electrodes are related to the high percentage of iron atoms as seen in the EDX findings [43]. In summary, the XRD analysis shows that the graphite electrode is trigonal, the main phase is the nickel face-centered cubic structure, while the G/$Ni_{\%95}Fe_{\%5}$ and G/$Ni_{\%95}Fe_{\%5}$-Ni(60s) electrodes are amorphous, and the G/$Ni_{\%95}Fe_{\%5}$-Ni(60s)(CV) electrode is crystalline.

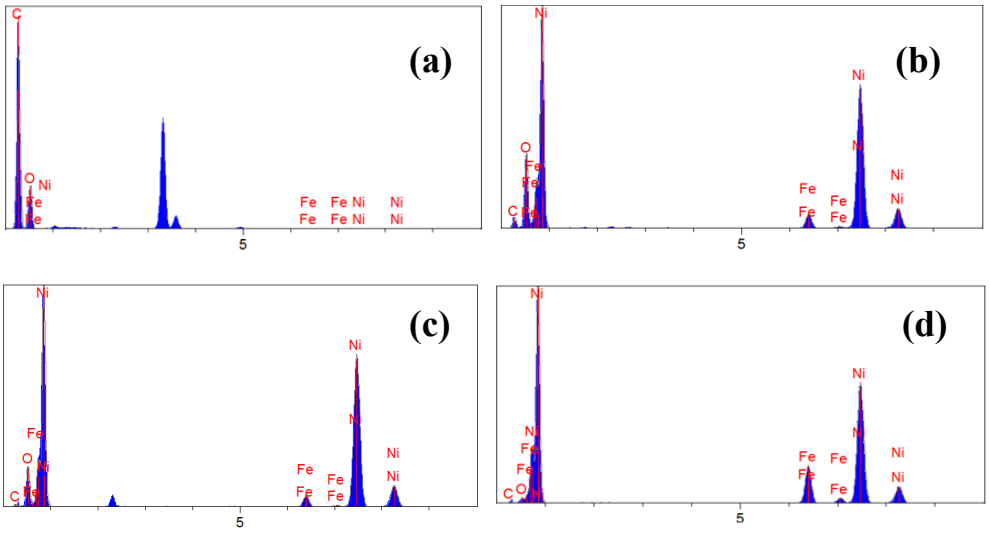

Figure 6. EDX spectrum of G (**a**), G/Ni%95Fe%5 (**b**), G/Ni%95Fe%5-Ni(60s) (**c**) and G/Ni%95Fe%5-Ni(60s)(CV) (**d**) of electrodes.

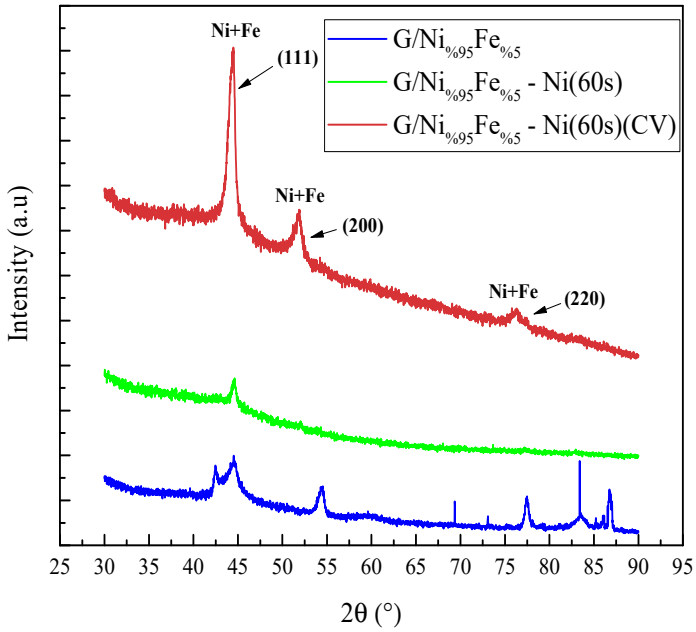

Figure 7. XRD pattern of G/Ni%95Fe%5 (---), G/Ni%95Fe%5-Ni(60s) (---), and G/Ni%95Fe%5-Ni(60s)(CV) (---) of electrodes (3° to 90°diffraction).

4. Conclusions

This study successfully demonstrates the development of a cost-effective and scalable electrocatalyst by modifying nickel-iron (Ni-Fe) alloy coatings on graphite electrodes for an enhanced hydrogen evolution reaction (HER) performance. By systematically investigating the impact of nickel modification on Ni-Fe alloys, the study addresses key limitations, such as the conductivity reduction caused by iron oxidation, and establishes an optimal modification duration of 60 s. The G/Ni%95Fe%5-Ni(60s) electrode exhibited a superior catalytic activity, achieving lower overpotentials, higher current densities, and increased hydrogen production efficiency compared to other compositions and modification durations.

The synergistic effects of nickel modification significantly improved the accessibility of active sites and HER kinetics, providing valuable insights into tailoring Ni-Fe-based electrocatalysts. These findings pave the way for the large-scale application of Ni-Fe alloys as robust and economically viable electrocatalysts in alkaline water electrolysis systems. Future studies can further optimize composition, morphology, and modification parameters to advance industrial-scale hydrogen production technologies.

Author Contributions: In this study, A.T. worked as a researcher and S.T.D. worked as a consultant. Laboratory studies were carried out by A.T. The planning of the study and the evaluation of the analyses were carried out by S.T.D. Writing, literature review, reading and compiling the article were carried out jointly. All authors have read and agreed to the published version of the manuscript.

Funding: This research received no external funding.

Data Availability Statement: Data sharing is not done.

Acknowledgments: The authors are very grateful to the Mardin Artuklu University Research Fund Office for financial support (Project number: MAÜ.BAP.23.SBF.012). We are very grateful to Murat FARSAK for his advice. We thank Sibel Derviş for her support.

Conflicts of Interest: We declare that the article is original, has been written by the stated authors, who are all aware of its content and approve its submission, and that no conflicts of interest exist, or if such conflicts exist, their exact nature must be declared. If accepted, it will not be published elsewhere in the same form, in English or in any other language, without the written consent of the publisher.

References

1. Iyer, R.K.; Prosser, J.H.; Kelly, J.C.; James, B.D.; Elgowainy, A. Life-cycle analysis of hydrogen production from water electrolyzers. *Int. J. Hydrogen Energy* **2024**, *81*, 1467–1478. [CrossRef]
2. Smit, R.; Helmers, E.; Schwingshackl, M.; Opetnik, M.; Kennedy, D. Greenhouse Gas Emissions Performance of Electric, Hydrogen and Fossil-Fuelled Freight Trucks with Uncertainty Estimates Using a Probabilistic Life-Cycle Assessment (pLCA). *Sustainability* **2024**, *16*, 762. [CrossRef]
3. Ahmed, S.; Yoon, W.; Jo, H.; Irshad, M.; Khan, M.K.; Kim, J. Structure-activity relationship and deactivation behavior of iron oxide during CO2 hydrogenation. *Chem. Eng. J.* **2024**, *499*, 156104. [CrossRef]
4. Ahmed, S.; Sugiarto, J.R.; Yoon, W.; Irshad, M.; Jo, H.; Bibi, S.S.; Kim, S.K.; Khan, M.K.; Kim, J. High-yield pentanes-plus production via hydrogenation of carbon dioxide: Revealing new roles of zirconia as promoter of iron catalyst with long-term stability. *J. Energy Chem.* **2025**, *102*, 431–442. [CrossRef]
5. Sadeq, A.M.; Homod, R.Z.; Hussein, A.K.; Togun, H.; Mahmoodi, A.; Isleem, H.F.; Patil, A.R.; Moghaddam, A.H. Hydrogen energy systems: Technologies, trends, and future prospects. *Sci. Total Environ.* **2024**, 173622. [CrossRef] [PubMed]
6. Yang, N.; Deng, J.; Wang, C.; Bai, Z.; Qu, J. High pressure hydrogen leakage diffusion: Research progress. *Int. J. Hydrogen Energy* **2024**, *50*, 1029–1046. [CrossRef]
7. Hannah, L. Chapter 21—Mitigation: Reducing greenhouse gas emissions, sinks, and solutions. In *Climate Change Biology*, 3rd ed.; Hannah, L., Ed.; Academic Press: Cambridge, MA, USA, 2022; pp. 439–472.
8. López, C.R.; Garcés, L.F.P.; Tepordei, D.; Moreno, S.P.; Šljukić, B.; Santos, D.M. Challenges in scaling low-carbon hydrogen production in Europe. In *Solar-Driven Green Hydrogen Generation and Storage*; Elsevier: Amsterdam, The Netherlands, 2023; pp. 287–319.

9. Balat, M. Potential importance of hydrogen as a future solution to environmental and transportation problems. *Int. J. Hydrogen Energy* **2008**, *33*, 4013–4029. [CrossRef]
10. Rasul, M.G.; Hazrat, M.A.; Sattar, M.A.; Jahirul, M.I.; Shearer, M.J. The future of hydrogen: Challenges on production, storage and applications. *Energy Convers. Manag.* **2022**, *272*, 116326. [CrossRef]
11. Ji, M.; Wang, J. Review and comparison of various hydrogen production methods based on costs and life cycle impact assessment indicators. *Int. J. Hydrogen Energy* **2021**, *46*, 38612–38635. [CrossRef]
12. Veziroğlu, T.N.; Şahin, S. 21st Century's energy: Hydrogen energy system. *Energy Convers. Manag.* **2008**, *49*, 1820–1831. [CrossRef]
13. Boundy, R.G.; Diegel, S.W.; Wright, L.L.; Davis, S.C. *Biomass Energy Data Book: Edition 4 (No. ORNL/TM-2011/446)*; Oak Ridge National Lab. (ORNL): Oak Ridge, TN, USA, 2011.
14. Hassan, Q.; Sameen, A.Z.; Salman, H.M.; Jaszczur, M.; Al-Jiboory, A.K. Hydrogen energy future: Advancements in storage technologies and implications for sustainability. *J. Energy Storage* **2023**, *72*, 108404. [CrossRef]
15. Ozturk, M.; Dincer, I. A comprehensive review on power-to-gas with hydrogen options for cleaner applications. *Int. J. Hydrogen Energy* **2021**, *46*, 31511–31522. [CrossRef]
16. Khetkorn, W.; Rastogi, R.P.; Incharoensakdi, A.; Lindblad, P.; Madamwar, D.; Pandey, A.; Larroche, C. Microalgal hydrogen production—A review. *Bioresour. Technol.* **2017**, *243*, 1194–1206. [CrossRef] [PubMed]
17. Demirci, U.B.; Miele, P. Overview of the relative greenness of the main hydrogen production processes. *J. Clean. Prod.* **2013**, *52*, 1–10. [CrossRef]
18. Idriss, H. Hydrogen production from water: Past and present. *Curr. Opin. Chem. Eng.* **2020**, *29*, 74–82. [CrossRef]
19. El-Shafie, M. Hydrogen production by water electrolysis technologies: A review. *Results Eng.* **2023**, 101426. [CrossRef]
20. Smolinka, T. *Fuels–Hydrogen Productıon | Water Electrolysis. Reference Module in Chemistry, Molecular Sciences and Chemical Engineering, Encyclopedia of Electrochemical Power Sources*; Fraunhofer Institute for Solar Energy Systems ISE: Freiburg, Germany, 2009; pp. 394–413.
21. Jan, B.M.; Dahari, M.B.; Abro, M.; Ikram, R. Exploration of waste-generated nanocomposites as energy-driven systems for various methods of hydrogen production; A review. *Int. J. Hydrogen Energy* **2022**, *47*, 16398–16423.
22. Ahmad, Z. *Basic Concepts in Corrosion. Principles of Corrosion Engineering and Corrosion Control*; Elsevier: Amsterdam, The Netherlands, 2006; pp. 9–56.
23. Wei, L.; Tian, N.; Zhou, Z.-Y.; Jiang, Y.-X.; Sun, S.-G. Electrocatalyst Preparation by Electrodeposition. In *Encyclopedia of Interfacial Chemistry, Surface Science and Electrochemistry*; Elsevier: Amsterdam, The Netherlands, 2018; pp. 507–520.
24. Wang, S.; Lu, A.; Zhong, C.J. Hydrogen production from water electrolysis: Role of catalysts. *Nano Converg.* **2021**, *8*, 4. [CrossRef] [PubMed]
25. Xiong, T.; Zhu, Z.; He, Y.; Balogun, M.S.; Huang, Y. Phase evolution on the hydrogen adsorption kinetics of NiFe-based heterogeneous catalysts for efficient water electrolysis. *Small Methods* **2023**, *7*, 2201472. [CrossRef] [PubMed]
26. Hong, S.H.; Ahn, S.H.; Choi, J.; Kim, J.Y.; Kim, H.Y.; Kim, H.-J.; Jang, J.H.; Kim, S.K. High-activity electrodeposited NiW catalysts for hydrogen evolution in alkaline water electrolysis. *Appl. Surf. Sci.* **2015**, *349*, 629–635. [CrossRef]
27. Valdez, T.I.; Munster, J.; Miller, E.; Freund, S. Supply processes and machinery. In *Machinery and Energy Systems for the Hydrogen Economy*; Elsevier: Amsterdam, The Netherlands, 2022; pp. 191–213.
28. Rodriguez, C.A.D.; Tremiliosi-Filho, G. Electrochemical Deposition. In *Encyclopedia of Tribology*; Wang, Q.J., Chung, Y.W., Eds.; Springer: Boston, MA, USA, 2013; pp. 918–922.
29. Topak, A Nikel Modifiye Nikel-Demir Kaplı Grafit Elektrodun Karakterizasyonu ve Bazik Ortamdaki Katalitik Etkisi. Master's Thesis, Mardin Artuklu University, Mardin, Türkiye, 2024.
30. Gu, S.; Xu, B.; Yan, Y. Electrochemical energy engineering: A new frontier of chemical engineering innovation. *Annu. Rev. Chem. Biomol. Eng.* **2014**, *5*, 429–454. [CrossRef] [PubMed]
31. Harada, Y.; Hua, Q.; Harris, L.C.; Yoshida, T.; Gewirth, A.A. Electrodeposition of Fractal Structured Nickel for Hydrogen Evolution Reaction in Alkaline. *ChemElectroChem* **2024**, e202400005. [CrossRef]
32. Fathyunes, L.; Muilwijk, C.; Brabazon, D. Hydrothermal synthesis of (NiFe/NiCo) S@ NF bilayer electrocatalyst for efficient hydrogen evolution reaction. *Int. J. Hydrogen Energy* **2024**, *78*, 622–633. [CrossRef]
33. Wen, J.; Lee, M.S. Recovery of nickel and cobalt metal powders from the leaching solution of spent lithium-ion battery by solvent extraction and chemical reduction. *Miner. Process. Extr. Metall. Rev.* **2024**, *45*, 415–425. [CrossRef]
34. Kim, J.; Jung, H.; Jung, S.M.; Hwang, J.; Kim, D.Y.; Lee, N.; Kim, K.S.; Kwon, H.; Kim, Y.T.; Han, J.W.; et al. Tailoring binding abilities by incorporating oxophilic transition metals on 3D nanostructured Ni arrays for accelerated alkaline hydrogen evolution reaction. *J. Am. Chem. Soc.* **2020**, *143*, 1399–1408. [CrossRef] [PubMed]
35. Jia, P.; Lan, X.; Li, X.; Wang, T. Highly selective hydrogenation of furfural to cyclopentanone over a NiFe bimetallic catalyst in a methanol/water solution with a solvent effect. *ACS Sustain. Chem. Eng.* **2019**, *7*, 15221–15229. [CrossRef]
36. Zhou, X.; Zi, Y.; Xu, L.; Li, T.; Yang, J. Core–shell-structured prussian blue analogues ternary metal phosphides as efficient bifunctional electrocatalysts for oer and her. *Inorg. Chem.* **2021**, *60*, 11661–11671. [CrossRef] [PubMed]

37. Abdollahi, A.; Ghaffarinejad, A.; Arabi, M. Electrodeposition of Ni-Fe on graphite rod as an efficient and binder-free electrocatalyst for oxygen and hydrogen evolution reactions. *J. Alloys Compd.* **2023**, *937*, 168400. [CrossRef]
38. Li, D.; Liu, H.; Feng, L. A review on advanced FeNi-based catalysts for water splitting reaction. *Energ Fuel* **2020**, *34*, 13491–13522. [CrossRef]
39. Telli, E.; Döner, A.; Kardaş, G. Electrocatalytic oxidation of methanol on Ru deposited NiZn catalyst at graphite in alkaline medium. *Electrochim. Acta* **2013**, *107*, 216–224. [CrossRef]
40. Aydın, Ö.; Atilla, P.; Akben, S.B.; Farsak, M. Preparation of green hydrogen catalyst with multi-objective optimization. *Mol. Catal.* **2022**, *529*, 112544. [CrossRef]
41. Topak, A.; Toprak Döşlü, S. Characterisation of a graphite electrode coated with a nickel-modified nickel-iron alloy and catalytic effect in an alkaline medium. In Proceedings of the Eighth International Hydrogen Technologies Congress (IHTEC 2024), Diyarbakir, Turkiye, 12–15 May 2024.
42. Jo, W.; Jeong, D.; Jeong, J.; Kim, T.; Han, S.; Son, M.; Kim, Y.; Park, Y.H.; Jung, H. Electrocatalytic properties of pulse-reverse electrodeposited nickel phosphide for hydrogen evolution reaction. *Front. Chem.* **2021**, *9*, 781838. [CrossRef] [PubMed]
43. Messaoudi, Y.; Belhadj, H.; Khelladi, M.R.; Azizi, A. Rational design of NiFe alloys for efficient electrochemical hydrogen evolution reaction: Effects of Ni/Fe molar ratios. *RSC Adv.* **2022**, *12*, 29143–29150. [CrossRef] [PubMed]
44. Hançer, H.; Telli, E.; Farsak, M. The catalytic effect of trimetallic alloy modified C-felt electrodes on hydrogen evolution reaction. *Int. J. Hydrogen Energy* **2022**, *47*, 25145–25154. [CrossRef]
45. Zhu, Y.; Liu, T.; Li, L.; Song, S.; Ding, R. Nickel-based electrodes as catalysts for hydrogen evolution reaction in alkaline media. *Ionics* **2018**, *24*, 1121–1127. [CrossRef]
46. Farmani, A.A.; Nasirpouri, F. Boosting hydrogen and oxygen evolution reactions on electrodeposited nickel electrodes via simultaneous mesoporosity, magnetohydrodynamics and high gradient magnetic force. *J. Mater. Chem. A* **2020**, *8*, 24782–24799. [CrossRef]
47. Vaze, A.S.; Sawant, S.B.; Pangarkar, V.G. Electrochemical oxidation of isobutanol to isobutyric acid at nickel oxide electrode: İmprovement of the anode stability. *J. Appl. Electrochem.* **1997**, *27*, 584–588. [CrossRef]
48. Navarro-Flores, E.; Chong, Z.; Omanovic, S. Characterization of Ni, NiMo, NiW and NiFe electroactive coatings as electrocatalysts for hydrogen evolution in an acidic medium. *J. Mol. Catal. A Chem.* **2005**, *226*, 179–197. [CrossRef]
49. Shi, B.; Li, C.; Han, R.; Li, Q.; Li, P.; Chen, X. Single-Step Synthesis of Nanocrystalline Fe-Ni/Fe-Co-Ni Magnetic Alloy Coating via Directional Plasma Spray. *Materials* **2023**, *16*, 2544. [CrossRef] [PubMed]

Disclaimer/Publisher's Note: The statements, opinions and data contained in all publications are solely those of the individual author(s) and contributor(s) and not of MDPI and/or the editor(s). MDPI and/or the editor(s) disclaim responsibility for any injury to people or property resulting from any ideas, methods, instructions or products referred to in the content.